ISSN 0252-1075
Contribution from IITM
Research Report No. RR-115

Termination of Indian Ocean Dipole Event in an Ocean General Circulation Model

Bijoy Thompson, C. Gnanaseelan, Anant Parekh
and
P. S. Salvekar

MARCH 2007

Indian Institute of Tropical Meteorology
Dr. Homi Bhabha Road, Pashan Pune - 411 008
Maharashtra, India

E-mail : lip@tropmet.res.in Fax : 91-020-25893825
Web : http://www.tropmet.res.in Telephone : 91-020-25893600

CONTENTS

Abstract

1.	**Introduction**	**1**
2.	**Model and Data**	**3**
3.	**Results and Discussion**	**6**
	3.1 Model Simulation of Climatological Features	**6**
	3.2 Surface and Subsurface Temperature Variability in the Tropical Indian Ocean	**6**
	3.3 Evolution of SST Anomalies over EEIO	**8**
	3.4 Processes Associated with IOD Termination	**9**
	3.5 Heat Budget	**11**
	3.6 Thermocline Depth Anomalies	**12**
4.	**Summary**	**13**
5.	**Acknowledgements**	**14**
6.	**References**	**15**
7.	**Figures**	**18**

Termination of Indian Ocean Dipole Event in an Ocean General Circulation Model

Bijoy Thompson, C. Gnanaseelan, Anant Parekh and P. S. Salvekar
Indian Institute of Tropical Meteorology, Pune, India

ABSTRACT

The Modular Ocean Model Version 4 has been used to study the oceanic processes associated with the termination of Indian Ocean Dipole (IOD) mode events in the tropical Indian Ocean. An ocean general circulation model tuned for Indian Ocean, forced by interannually varying surface forcing has been first validated with the available observations and the model simulated oceanic parameters are compared with the existing assimilation products. The climatological temperature and circulation features of the Indian Ocean are well reproduced by the model. Good agreement is found between the seasonal sea surface temperature (SST) climatologies of model and Levitus (1998), with rms differences of 0.37, 0.26, 0.37 and 0.31^{o}C for winter (December-February), spring (March-May), summer (June-August) and fall (September-November) seasons respectively. The surface and subsurface temperature variabilities in the tropical Indian Ocean also are well captured by the model. The model successfully simulated the cooling/warming trend observed in the region during dipole mode years. The heat budget analysis of the model simulated fields revealed that positive surface heat flux and vertical advection have played a dominant role in the termination of IOD co-occurring with El-Nino, where as horizontal and vertical advections are responsible for IOD termination during non El Nino years. The contribution of surface heat flux is significant during the initial phase of termination during all dipole years. The dipole termination during the negative dipole year 1996 was mainly caused by the anomalous negative surface heat fluxes and horizontal advective processes.

1. Introduction

The Indian Ocean Dipole/Zonal (IOD) mode events (Saji et al., 1999; Webster et al., 1999; Annamalai and Murtugudde, 2004 for a review) have widely gained attention because of its impacts on global and regional climate variability (Zubair et al., 2003; Behera and Yamagata, 2003; Saji and Yamagata, 2003). Kripalani and Kumar (2004) showed the direct influence of IOD on northeast monsoon rainfall variability over India. Kripalani et al. (2005) investigated the influence of IOD on extreme rainfall events over East Asia. The relationship between Indian summer monsoon and IOD is studied by Kulkarni et al. (2006). Their study revealed that Indian monsoon had more influence on IOD than vice-a-versa. IOD events are characterized by strong temperature anomalies in the southeastern tropical Indian Ocean and relatively weak temperature anomalies in the western tropical Indian Ocean. These temperature anomalies depict a dominant mode of interannual basin scale Sea Surface Temperature (SST) variability in the Indian Ocean (Saji et al., 1999). The SST variability in the Indian Ocean has been extensively discussed through several studies (Nicholls, 1989; Behera et al., 1999 and 2000; Yu and Reinecker, 1999 and 2000; Murtugudde et al., 2000; Iizuka et al., 2000; Vinayachandran et al., 2002). Rao et al., (2002) studied the subsurface variability in the tropical Indian Ocean and suggested that the dominant mode of interannual variability in the tropical Indian Ocean is characterised by the dipole structure. Shinoda et al., (2004) discussed the surface and subsurface dipole variability in the Indian Ocean. Rao and Behera (2005) discussed the subsurface influence on SST in the tropical Indian Ocean, its variability and relationship with ENSO and IOD events.

Murtugudde et al., (2000) discusses the role of surface heat fluxes in the termination 1997 IOD event. Rao and Yamagata (2004) discuss the possible role of downwelling Kelvin waves in IOD termination. They observed significant intraseasonal oscillations are associated with equatorial westerly winds prior to the termination of IOD events and they suggested that the anomalous downwelling Kelvin wave excited by these westerlies leads to the termination of SST anomalies in the East Equatorial Indian Ocean (EEIO).

During all strong IOD years the cooling/warming is vigorous over EEIO but the region of western warming shows large variability from event to event

(Annamalai and Murtugudde, 2004). The characteristic feature of the IOD events is the SST variability over EEIO, which is one of the regions where Bjerkness (1969) feedbacks occur due to interactions between the thermocline and SST (Annamalai and Murtugudde, 2004). The importance of EEIO in the initiation and termination of IOD events is well documented (Annamalai et al. 2003; Rao and Yamagata, 2004). Rao and Behera, (2005) discuss the importance of EEIO in representing the interannual variability in Indian Ocean. Here we defined positive (negative) IOD termination as the disappearance of negative (positive) SST anomalies over the EEIO. The tropical Indian Ocean experienced three intense positive IOD events during 1961, 1994 and 1997. In these three IOD events 1961 occurred with ENSO and 1994 event occurred with the existence of a very weak ENSO phenomenon in the Pacific and 1997 IOD event co-occurred with strong ENSO. This study is focused on the strong EEIO cooling events occurred in 1961, 1994 and 1997. Figure 1 shows the composite evolution of SST anomalies over EEIO (90^{o}E to 110^{o}E, 10^{o}S to Equator) for strong positive IOD years 1961, 1994 and 1997. The negative temperature anomalies after reaching the peak phase (September/October), starts decreasing more than one month before the actual surface IOD termination. A strong negative IOD year 1996 is also considered in this study to show the contrasting features. Previous studies on IOD termination have tried to understand the physical and dynamical processes during the collapse of IOD (or after the anomalies have been reversed). Also not many studies have focused on the processes associated with the initiation of termination processes (i.e., just before or when the cooling/warming trend over EEIO ceases). In the present study using an Ocean General Circulation Model (OGCM) simulation we address the dynamic and thermodynamic processes which initiate the termination of cooling (during positive IOD years) or warming (during negative IOD years) over EEIO. The discussions are based on the daily output from the model simulation for these IOD years. The heat budget analysis of upper ocean has been performed to understand the individual contributions from advective and heat flux components during the reversal of cooling (warming) trend. The report is organised as follows. Section 2 describes the model used for the study and the different datasets used for model forcing and analysis. Section 3.1 discusses the climatological SST and surface circulation simulated by the model. The temperature variability over tropical Indian Ocean is presented in section 3.2. Section 3.3 discusses the evolution of SST anomalies over the EEIO. Processes associated with IOD termination are discussed in Section 3.4. Section 3.5 and 3.6 discusses the heat budget and thermocline anomalies in the EEIO. Section 4 summarises the results.

2. Model and Data

The OGCM used in this study is the Geophysical Fluid Dynamics Laboratory (GFDL) Modular Ocean Model Version 4 (MOM4p0c) (Griffies et al., 2003). MOM is a finite difference version of the ocean primitive equations, which govern much of the large-scale ocean circulation. MOM is a z-coordinate (3 dimensional) numerical representation of hydrostatic primitive equations with Boussinesq approximation and explicit free surface. The horizontal coordinate used in the model is generalised orthogonal coordinate system. Prognostic variables include the two active tracers of temperature and salinity, the horizontal velocity components and passive tracer field, the height of free ocean surface. The time tendency for tracer and baroclinic velocity is discretised with a two-level forward step. The tracer and velocity are staggered in time, thus providing second order accuracy in time. The grid system is a rectangular Arakawa staggered B grid (Bryan, 1969) containing T cells and U cells. Within the T cell there is a T grid point, which defines the location of tracer quantities. Similarly each U cell contains a U grid point, which defines the location of zonal and meridional velocity components. The time stepping scheme is based on predictor-corrector method, which is more stable than the leap-frog scheme. Top model cells have time dependent volume, thus allowing for conservative fresh water input. The sole external mode solver is a variant of Griffies et al., (2001) explicit free surface. The model tracer field, the baroclinic velocity and free surface height are time stepped with 9600 seconds. Since the tracer and baroclinic time steps are equal, total tracer is conserved in the model, except for time descretisation errors arising from the use of a time filtered surface height. The barotropic fields have a time step of 120 seconds. The tracer advection is handled through Sweby scheme, which is multi-dimensional flux limited scheme. The equation of state is based on more accurate one described by McDougall et al., (2003) than the linearised equation of state. The in situ density is a function of the local potential temperature, salinity and hydrostatic pressure including the baroclinic pressure, free surface pressure and applied pressure from the atmosphere and sea ice. Horizontal friction scheme is based on the shear-dependent Smagorinsky viscosity according to Griffies and Hallberg (2000). The vertical mixing in the model is handled through K Profile Parameterisation (KPP) Scheme (Large et al., 1994) having local and non-local mixing with Bryan-Lewis background diffusivity (Bryan and Lewis, 1979). The KPP mixing consists of oceanic mixing in the turbulent boundary layer near the surface under heat flux and wind driven conditions and

relatively weak diapycnal mixing in the ocean interior due to internal waves, shear instability and double diffusion. The oceanic boundary layer depth is determined by the parameterisation of turbulent shear in terms of the bulk Richardson number. The important feature of the KPP scheme is the capability of the boundary layer to penetrate well into a stable thermocline in both convective and wind driven conditions. Bottom topography in the model is represented using the partial cells of Pacanowski and Gnanadesikan (1998). The overflow scheme of Campin and Goose (1999) has been implemented. It allows gravitationally unstable fluid parcels to move downslope through an upwind advection scheme. The heating due to penetrative shortwave radiation is attenuated by the inclusion of chlorophyll data.

The model region is 30^{o}E to 120^{o}E and 40^{o}S to 25^{o}N having 30 vertical levels. The upper ocean mixed layer and thermocline zones are well resolved in the model with 15 vertical levels within a depth of 155 m. The vertical resolution gradually changes to maximum thickness of 712 m at 5600 m. The model has been provided with realistic topography of 0.5^{o} resolution, which is derived from the 5-minute global topography ETOPO5 (Earth Topography-5minute) database. Model has a constant zonal resolution of 1^{o} and meridional resolution varying from 0.3353^{o} at equator to 0.7^{o} at 25^{o}N and 1.5^{o} at 40^{o}S. Solid walls are assumed at the eastern and southern boundaries and no slip conditions are assumed for momentum. For temperature and salt no flux boundary conditions are assumed. Additionally, the southern and eastern boundaries are provided with a sponge layer of 4^{o} width, where the temperature and salinity are restored to monthly climatologies of Levitus (1998). Within the sponge layer a Newtonian damping (5 days) is applied to the tracer equations. There is no mass flux through bottom and also insulating condition for heat and salt. The model was initialized using the annual climatologies of temperature and salinity from Levitus (1998) and forced with climatological downwelling shortwave and longwave radiation, 10m surface wind fields, specific humidity, air temperature, surface pressure and surface precipitation from NCAR climatology (Large and Yeager, 2004). Chlorophyll-a climatology computed from SeaWiFS satellite for the period 1999-2001 is provided to handle short wave penetration. After 20 years of spin up the model has been integrated for a period of 43 years from 1958-2000 with NCAR corrected interannual datasets (Large and Yeager, 2004) of daily downwelling shortwave and longwave radiation, six-hourly varying 10m surface wind fields, specific humidity, air temperature, surface pressure and monthly precipitation.

During the interannual simulation the surface fluxes are corrected on 30 day timescale using seasonal climatological SST and sea surface salinity. The basin wide average of this correction term during the simulation period for heat flux is smaller than -10 W/m^2 to +6 W/m^2 and for fresh water flux is -2.5x10^{-9} to + 0.5x10^{-9} m/s. The 43 year mean of heat flux correction shows 84% area of the basin within the range -5 to +5 W/m^2 and 10% area within the range -5 to -7 W/m^2 and +5 to +7 W/m^2. The head bay, western Arabian Sea and around Madagascar show the flux correction above ±5 W/m^2. The heat flux correction above +10 W/m^2 is seen only in the Persian Gulf. Even in the key regions having large interannual variability like EEIO, the correction term is observed to be very small. During the anomalous years 1961, 1994 and 1997 the heat flux correction term is found to be within ±10 W/m^2. We selected 10 W/m^2 as the threshold heat flux correction value because even if there is a continuous influx of 10 W/m^2 for one month (i. e, model relaxation time), it will lead to a rise of SST by 0.129^{o}C only. This suggests that the model temperature tendency above 0.129^{o}C/month can be considered reasonable. The low heat flux correction values emphasis that the thermodynamics of the model will not be deviated much from the real ocean due to the restoring. For the fresh water flux 85% area of the basin shows correction less than -0.2 x 10^{-7} to +0.2 x 10^{-7} m/s and 12% area in the range -0.2 to -0.5 x 10^{-7} m/s and +0.2 to +0.5 x 10^{-7} m/s. Fresh water flux corrections above ±0.2 x 10^{-7} m/s are seen only in the east and west Bay of Bengal regions. These low values of flux corrections imply that the model interannual simulations are not significantly affected by the weak sea surface temperature and the sea surface salinity restoring terms.

The Simple Ocean Data Assimilation (SODA) datasets are used for comparison with model simulations. The SODA version used here is SODA_1.2, which is a University of Maryland reanalysis product using an eddy-permitting global model based initially on POP_1.3 numerics and SODA procedure (Carton et al., 2005; Carton and Giese, 2006). For the validation and comparison of model simulated SST, HadISST v.1.1 is used. In situ sea surface observations and satellite derived estimates at the sea surface are included in the HadISST Global Ocean Surface Temperature analysis (Rayner et al., 2003).

3. Results and Discussion

3.1 Model Simulation of Climatological Features

The model simulations are validated with available observations before studying the interannual variability and mechanisms involved in the decay of IOD events. The model climatology is calculated for the entire simulation period from 1958-2000. The difference between the seasonal SST climatologies of model and Levitus is given in figure 2. The model SST shows an RMS difference of 0.37, 0.26, 0.37 and 0.31^{o}C for winter (December-February), spring (March-May), summer (June-August) and fall (September-November) seasons with Levitus (1998) seasonal climatology and 0.25^{o}C with the annual climatology. The climatological features like winter cooling in the northern Arabian Sea, the pre-monsoon warming in northern Indian Ocean and monsoonal cooling in western Arabian Sea are well simulated by the model. The current climatology from model simulation is compared with SODA climatological currents, which is also available for the same period. The existence of strong eastward flowing equatorial jet, during the transition periods April/May and October/November is well simulated by model and is comparable with SODA datasets. Equatorial Jets of magnitude 0.7m/s during spring and fall season were observed in the SODA climatology. The Wyrtki Jets simulated by the model during spring season also show magnitude of about 0.7m/s between 70^{o}E and 80^{o}E and fall jets have magnitude of about 0.55 m/s between 60^{o}E to 70^{o}E. However the observations show the jets of magnitude 0.8 m/s during spring and 0.9 m/s during fall. The climatological and interannual simulation of surface and subsurface temperature and currents from the model simulation is described in Thompson et al., (2005). The weakening of fall jets in OGCM simulations is described by many authors (Schott and McCreary, 2001; Han et al. 1999). However the spatial pattern of the jets in model simulations agrees well with the observational studies by Reverdin (1987) and Hastenrath and Greischer (1991). The climatological features of circulation and salinity over the tropical Indian Ocean and its variability during the IOD years from the model simulations are discussed in Thompson et al., (2006).

3.2 Surface and Subsurface Temperature Variability in the Tropical Indian Ocean

The IOD events can be represented with a simple time series index called Dipole Mode Index (DMI). The DMI is defined as the difference between the SST anomalies in the western equatorial Indian Ocean (50^{o}E to 70^{o}E, 10^{o}S to 10^{o}N)

and the southeastern tropical Indian Ocean (90^{o}E to 110^{o}E, 10^{o}S to the Equator) (Saji et al. 1999). The DMI derived from the model, HadISST, and SODA data sets are shown in figure 3. The model has simulated the recent positive IOD events (1961, 1963, 1967, 1972, 1977, 1982, 1994 and 1997) and negative IOD events (1958, 1960, 1964, 1975, 1984, 1989, 1992 and 1996) very well. The model DMI compares very well with the DMI calculated from HadISST. For 1961, both the model and SODA overestimate the DMI.

The leading Empirical Orthogonal Function (EOF) of Sea Surface Temperature Anomaly (SSTA) from model and HadISST are shown in figure 4. The EOF analysis of monthly SSTA shows that the SST variability in the Indian Ocean is mainly described by the first two modes. The EOF1 of model and HadISST explain 37% and 39% of total variability respectively, which is of uniform polarity in the entire tropical Indian Ocean. This mode corresponds to ENSO variability (Saji et al., 1999). The second mode gives 14% of total variability for model and 8% for HadISST. The second mode corresponds to a dipole mode with opposite loadings in southeastern tropical Indian Ocean and western tropical Indian Ocean. However EOF1 and EOF2 of the model seasonal SSTA is characterised by the dipole structure during fall showing 36% and 33% of total variability (figures not shown). During winter season also the EOF1 (50%) and EOF2 (12%) are marked by zonal dipole structure, but the opposite loading in the southeastern tropical Indian Ocean is seen further southward in EOF1. The EOF1 for spring (58%) and summer (49%) seasons have uniform polarity over the entire Indian Ocean. The EOF2 (10%) during spring season is noted by a north-south dipole structure having positive loading south of 5^{o}S and negative loading north of 5^{o}S. The zonal dipole structure is also evident in the EOF2 during summer season showing 15% of total variability. The EOF analysis of SSTA illustrates that in seasonal time scale the SST variability in the Indian Ocean is dominated by ENSO during spring and summer. However the IOD variability is prevailing during fall and winter seasons.

Earlier studies revealed that the dominant mode of interannual variability of the upper ocean heat content and sea level in the tropical Indian Ocean is marked by a zonal dipole structure (Rao et al., 2002). The EOF analysis of model temperature anomalies in the subsurface (80 m) shows that EOF1 is characterised by a dipole structure having 38% of total variability (figure 5). Further, it is noted that the maximum positive loading in the western Indian Ocean is not located at the

equator; it is seen south of the equator. A similar dipole structure is also seen in the EOF1 of model D20 (20 degree isotherm depth) anomalies, which explains 33% of total variability (figures not shown). These results are consistent with Rao et al. (2002). The subsurface temperature variability associated with dipole can be explained more effectively through the EOF analysis of temperature anomaly in the longitude-depth section along the equatorial belt (average over 10^{o}S - 5^{o}N). The leading mode of EOF is distinguished by the dipole structure, which explains 51% of total variability (figure 5). The maximum amplitude of this variability is observed around at 80 m depth. The leading EOF during spring, summer, fall and winter seasons show dipole structure explaining respectively 51%, 50%, 59% and 66% of the total variability (figure 6). The strongest loading is seen around 100^{o}E-105^{o}E in the EEIO and around 60^{o}E-70^{o}E in the western part. Similar features are also discussed in the OGCM study by Shinoda et al., (2004). This leading mode of EOF is referred as subsurface dipole mode in the Indian Ocean (Shinoda et al., 2004). The EOF analysis of model temperature anomalies reveals that the ENSO mode is dominant in the surface, while the subsurface temperature variability is largely governed by the zonal dipole mode in the tropical Indian Ocean.

3.3 Evolution of SST Anomalies over EEIO

The composite of SST anomalies over the EEIO from model (continuous line) and SODA (dashed line) for strong positive IOD years 1961, 1994 and 1997 are plotted in figure 1. The model composite anomalies show close agreement with SODA anomalies. The seasonal phase locking is one important characteristic of IOD events. The composite SST anomalies show fall in SST from May-June and the anomalies observed to be maximum in September-October. Maximum SST anomalies about 1.3^{o}C during September-October are shown in the composite analysis. Thereafter negative SST anomalies decreases leading to the collapse of IOD. The IOD events show clear variability in its time of origin, peak phase and termination. So we have done the comparison between SST anomalies of different data sets used in the study. The monthly evolution of model SST anomalies over the EEIO for 1961, 1994, 1996 and 1997 are compared with SODA and HadISST anomalies (figure 7). Though the composite evolution of model SST anomalies compares well with SODA data, in individual years some differences are seen between these two datasets as seen in figure 7. During 1961 and 1994 both the model and SODA overestimates the cooling over the EEIO. In September 1996 the

HadISST shows a decrease in positive SST anomaly, this cooling event is not seen in model or SODA data sets. The EEIO cooling in 1997 is also well evident in the model simulation.

3.4 Processes Associated with IOD termination

The subsurface temperature anomalies in the EEIO during positive (negative) IOD events are stronger than the associated surface cooling (warming). These subsurface temperature anomalies are seen up to 150m in the model simulations. During 1961 and 1997 the model shows negative subsurface anomalies of 5-6^{o}C in the EEIO (figure 8). In 1994 the temperature anomalies in the EEIO are about 4^{o}C. During 1996 the EEIO shows subsurface warming of about 4^{o}C in November. The model simulations showed maximum cooling during the positive IOD years at a depth of about 70-80m, in contrast maximum warming during negative IOD years occurs at about 120m. Strong upwelling is observed in the EEIO during positive IOD years (May-June in 1994 and 1961 and June in 1997), which brings cold subsurface water near Sumatra coast. In contrast to the positive IOD years, during 1996 equatorial Indian Ocean was distinguished by strong downwelling to the east of 85^{o}E during May. During 1961 and 1994 strong negative temperature anomalies observed in July. From July to December 1996 strong positive anomalies are seen at deeper level. However during July/August 1997 the subsurface anomalies are very weak and maximum anomalies are seen in November-December. The decay of surface and subsurface temperature anomalies in 1961 and 1994 are mainly due to the strong downwelling of warm surface water. Considerable downwelling is observed starting October in 1961 and September in 1994. The time-depth plot of temperature anomalies shows the advection of warm surface water downwards which cause decrease in negative temperature anomalies. However in 1997 no such signatures of organized downwelling process are observed in the termination phase of IOD.

The SST anomalies during the termination phase of 1961, 1994 and 1997 IOD years are shown in figure 9a. The vertical velocity (model) at 50m (figure 9c), surface wind speed (figure 9e) and latent heat flux (figure 9g) calculated from model SST is also indicated. All these parameters are averaged for the EEIO region. During 1961 IOD termination initiated on 30 September in the surface (figure 9a). The vertical velocity analysis reveals that the initial phase of IOD collapse is characterized by a reduction in upward vertical velocity (figure 9c). The positive

vertical velocity (upwelling) shows a drop and by mid October negative vertical velocity (downwelling) appears in the EEIO. The negative vertical velocity shows maximum magnitude during the end of November, thereafter it gradually decreases and by middle of December positive vertical velocity is seen in the region. Corresponding to the change in vertical velocity the SST anomalies shows a remarkable decrease (from -2.8^{o}C to -0.6^{o}C) from late September to early December. The rate of decrease in SST anomaly is observed to be weak during December. The surface wind speed also shows a reduction in magnitude from late September. The role of latent heat flux (LH) is not appeared to be so obvious during the termination of IOD (Figure 9g). However the LH shows an increase in magnitude from November onwards. The weak downwelling from early December, the appearance of upwelling currents by middle of December and the increased release of LH are responsible for the decrease in SST warming from early December. The negative SST anomalies disappeared from EEIO by July 1962 (figure not shown). During 1994 termination process started on 3 September at the surface and the surface dipole terminated completely from EEIO by December 21 (figure 9a). Resembling to the initial phase of termination in 1961, reduction in positive vertical velocity is observed in 1994 dipole termination (figure 9c). The maximum magnitude of negative vertical velocity observed during late November. Even though the release of LH shows a drop prior to the initiation of IOD termination, an increase in the heat loss through LH is observed in later stage. This explains that upwelling and reduction in heat loss through LH contributes during the initial phase of IOD termination, however the LH is not favorable for surface warming in the later stages. The IOD termination is primarily driven by ocean dynamics after the initiation of termination. In 1997 the termination process initiated at the surface on 16 November (figure 9a). A decrease in surface wind speed and corresponding reduction in LH release is noticed from early October in 1997. During 1997 the SST warming is largely driven by the LH rather than downwelling processes.

Contrasting features are evident in the negative dipole year 1996, where the termination process started on 2 October. The initiation is marked by an increase in surface wind speed and net heat loss through LH release (figure 9b, f and h). A decrease in surface wind speed and LH is seen in the EEIO from late October to late November. This reduced heat loss from ocean temporarily ceased the SST cooling during November. The strong winds in December helped for the termination the surface dipole by 6 December.

3.5 Heat budget

Heat budget analysis of the upper ocean has been carried out for understanding the individual contributions of horizontal and vertical advective processes and net surface heat flux for the heat content changes over STIO. The temperature tendency of the model (over a depth of H=50m) is calculated as

$$\frac{\partial T}{\partial t} = -\left(u\frac{\partial T}{\partial x} + v\frac{\partial T}{\partial y} + w\frac{\partial T}{\partial z} \right) + \frac{Q_S}{\rho C_p H} + Q_d \qquad ---------- \quad (1)$$

where $\left(u\frac{\partial T}{\partial x}, v\frac{\partial T}{\partial y} \; and \; w\frac{\partial T}{\partial z} \right)$ are the zonal, meridional and vertical advective terms, Q_S denotes the net surface heat flux and Q_d represents the diffusive terms. $\rho = 1026 \; kg/m^3$ is the mean density of the upper layer; $Cp = 3902 \, J/kg/K$ is the specific heat capacity of seawater.

The anomalies of model 50m heat content tendency, vertical advection, horizontal advection and net surface heat flux averaged over EEIO during 1961, 1994, 1996 and 1997 are shown in figure 10. In 1961 during the phase transition (cooling trend to warming), the model heat content tendency closely follows the vertical advection. Within a few days of initiation of termination heat content tendency became positive. The termination of IOD was initiated by the combined action of vertical advection, horizontal advection and surface heat flux. Even though positive heat flux anomalies are observed during the initial period of termination, the anomalies are considerably weak in magnitude from mid November. The heat budget analysis shows that the vertical and horizontal advection contributes substantially to the initiation and further decay of 1961 dipole event. The contribution of surface heat flux is very small after the initial phase of termination. After the reversal of cooling trend, vertical and horizontal advection aided the further decay of SST anomalies over EEIO. The heat budget components show similar features in 1994 also. The vertical and horizontal advection plays major role in the decay of negative temperature anomalies in 1994. During 1994 also the positive heat flux anomalies are considerable during the initial period of IOD termination. However the role of horizontal advection is negligible during 1997 IOD termination. The positive heat flux anomalies and vertical advection are found to be responsible for the IOD

termination process. This positive heat flux anomalies are largely contributed by the reduction in latent heat flux (figure 9g). A major difference in the termination of IOD between 1997 (ENSO year) and non ENSO years (1961 and 1994 (weak ENSO)) is the continuous influence of anomalous positive surface heat flux together with vertical advection during the entire termination period in 1997, whereas horizontal and vertical advection are dominant in the non El Nino years.

During 1996 the model heat content tendency shows reversing trend on September 23 and a couple of days after initiation of termination, the model heat content tendency became negative. Unlike positive IOD years, during 1996 the heat content tendency closely followed the surface heat flux anomalies. In November 1996 the SST anomalies shows mild warming over EEIO, which is mainly due to reduction in latent heat flux. This feature is reflected in heat budget analysis also. The variation in heat content tendency is appeared to be very small during November 1996. The role of vertical advection is observed to be insignificant during the initiation and further termination of 1996 IOD event. Also heat budget analysis demonstrates that contribution from horizontal advection is considerable in the termination of positive SST anomalies from EEIO.

3.6 Thermocline Depth Anomalies

The EEIO is characterised by rising of the thermocline (taken as the depth of 20^{o}C isotherm, D20) during positive IOD events and in negative IOD years it shows a deepening (Vinayachandran et al., 2002). The D20 anomalies during the termination phase of the above IOD events are shown in figure 11. The figure indicates that the shoaling (deepening) of thermocline continuous even after the termination process begins in the surface. During 1961 and 1994, more than one month after the beginning of surface IOD termination, the thermocline shows a deepening from early November. The variations in the thermocline represent the ocean dynamics rather than the thermodynamical processes. The deepening of the thermocline during 1961 and 1994 reflects the dominance of vertical advective processes in the termination of these IOD events. The thermocline shows a deepening of 25m in 1961 and 15m in 1994. However the deepening of thermocline after the initiation of termination was less prominent (<10m) in 1997. The shoaling of thermocline continues up to middle of December. The D20 shows a gradual deepening from Mid December onwards. The marginal variation of D20 anomalies

emphasis the major role of surface heat flux in the warming of upper ocean during 1997 IOD termination. During the negative IOD year (1996) the EEIO is marked by positive D20 anomalies. The deepening/raising of the thermocline was considerably small during the termination phase of IOD. This feature supports the earlier discussions that the contribution of vertical advection is negligible in 1996 IOD termination.

4. Summary

Indian Ocean versions of the MOM4 OGCM simulations are validated with available observations and are compared with the assimilated SODA datasets. The model SST shows an rms difference of 0.37, 0.26, 0.37 and 0.31^{o}C for winter, spring, summer and fall seasons respectively with Levitus (1998) seasonal climatology and 0.25^{o}C with the annual climatology. Without the use of any relaxation to observed interannual SST anomalies the model quantitatively reproduced the main features of the interannual variability like IOD. Despite the SST relaxation to seasonal climatology the standard deviation of the model heat budget anomaly imbalance is less than 10% (~20 W/m^2). Strong subsurface negative temperature anomalies are seen in the STIO from July in 1961 and 1994. In fact, during 1997 strong subsurface negative temperature anomalies are observed in October/November. The positive IOD years 1961, 1994 and 1997 shows significant variability in the initiation and mechanism of IOD termination. During 1961, 1994 and 1997 IOD termination has been initiated at surface on 30 September, 3 September and 16 November respectively. Heat budget analysis showed that during pure IOD years, 1961 and 1994, the vertical and horizontal advection plays major role in the initiation of termination and further collapse of IOD. The net surface heat flux is observed to be important in only during the initial phase of termination. However in 1997 positive net surface heat flux anomaly and vertical advection is the major contributor to the IOD collapse. The contribution of horizontal advection is negligible in 1997. During 1996, which is a negative IOD year, the dipole termination is initiated on 19 October in the surface. The combined action of negative surface heat flux anomalies and horizontal advection are observed to be important in the initiation of termination and further collapse of IOD during 1996.

Acknowledgments.

Bijoy Thompson is acknowledging CSIR, India for providing financial support for research work. We also acknowledge financial support of Department of Ocean Development, Govt. of India. The encouragement by Director, I.I.T.M. is sincerely acknowledged. We thank Dr. R.H. Kripalani for critical revision which helped to improve the manuscript. The authors acknowledge Dr. Stephen Griffies and Dr. P.S. Swathi for their support and discussions during model installation and integration. Acknowledgments are also due to GFDL, Princeton for making the MOM4 code available, NCAR, UMD, and UK Met. Office for datasets. Figures are drawn using Ferret.

REFERENCES

Annamalai, H. and R. Murtugudde. 2004. Role of the Indian Ocean in regional climate variability. In Earth Climate: The Ocean-Atmosphere Interaction, C. Wang, S.-P. Xie and J.A. Carton (eds.), AGU Geophysical Monograph, *147*, 213-246.

Annamalai H., R. Murtugudde, J. Potemra, S. P. Xie and B. Wang. 2003. Coupled Dynamics over Indian Ocean: spring initiation of the Zonal Mode, Deep Sea Res., Part II, *50*, 2305-2330.

Behera S.K., R. Krishnan and T. Yamagata. 1999. Unusual ocean-atmosphere conditions in the tropical Indian Ocean during 1994, Geophys. Res. Lett., *26*, 3001-3004.

Behera S. K., P. S. Salvekar and T. Yamagata. 2000. Simulation of Interannual SST variation in the tropical Indian Ocean, J. Clim., *13*, 3487-3489.

Behera S. K. and T. Yamagata. 2003. Impact of the Indian Ocean Dipole on the southern Oscillation, J. Meteorol. Soc. Japan., *81*, 169-177.

Bjerkness, J. 1969. Atmospheric teleconnections from equatorial Pacific, Mon. Weather Rev., *97*, 163-172.

Bryan, K. 1969. A numerical method for the study of the circulation of the world ocean, J. Comp. Phy., *4*, 347-376.

Bryan K. and L.J. Lewis. 1979. A water mass model of the world ocean, J. Geophys. Res., *84*, 2503–2517.

Campin J. M. and H. Goose. 1999. Parameterisation of density-driven downsloping flow for a coarse resolution ocean model in z-coordinate, Tellus, *51*, 412-430,

Carton J. A., B.S. Giese, and S.A. Grodsky. 2005. Sea level rise and the warming of the oceans in the Simple Ocean Data Assimilation (SODA) ocean reanalysis, J. Geophys. Res., *110*, No. C9, C0900610.1029/2004JC002817.

Carton J.A. and B.S. Giese. 2006. SODA: A reanalysis of ocean climate, Mon. Wea. Rev., (submitted).

Griffies S.M. and R.W. Hallberg. 2000. Biharmonic friction with a Smagorisky viscosity for use in large-scale eddy-permitting ocan models, Mon. Wea. Rev., *128*, 2935-2946.

Griffies S.M., R.C. Pacanowski, R.M. Schmidt and V. Balaji. 2001. Tracer conservation with an explicit free surface for z-coordinate ocean models, Mon. Wea. Rev., *129*, 1081-1098.

Griffies S.M., M.J. Harrison, R.C. Pacnowski and A. Rosati. 2003. A Technical Guide to MOM4. GFDL Ocean Group Technical Report No. 5, Princeton, NJ: NOAA/ Geophysical Fluid Dynamics Laboratory.

Han W., J.P. McCreary, D.L.T. Anderson and A. J. Mariano. 1999. On the dynamics of eastward surface jets in the equatorial Indian Ocean, J. Phys. Oceanogr., *29*, 2191-2209.

Hastenrath S. and L. Greischar. 1991. The monsoonal current regimes of the tropical Indian Ocean: observed surface flow fields and their geostrophic and wind-driven components. J. Geophys. Res., *96*, 12619-12633.

Kripalani R.H. and P. Kumar. 2004. Northeast monsoon rainfall variability over south peninsular India vis-a-vis the Indian Ocean Dipole Mode, Int. J. Climatol., 24, 1267–1282.

Kripalani R.H., J.H. Oh, J.H. Kang, S.S. Sabade and A. Kulkarni. 2005. Extreme monsoons over East Asia: Possible role of Indian Ocean Zonal Mode, Theor. Appl. Climatol. 82, 81–94.

Kulkarni A., S.S. Sabade and R.H. Kripalani. 2006. Association between extreme monsoons and the dipole mode over the Indian subcontinent Meteorol Atmos Phys., DOI 10.1007/s00703-006-0204-9.

Iizuka S., T. Matsuura and T. Yamagata. 2000. The Indian Ocean SST dipole simulated in a coupled general circulation model, Geophys. Res. Lett., *27*, 3369-3372.

Large W. G., J.C. McWilliams and S.C. Doney. 1994. Oceanic vertical mixing: A review and a model with a nonlocal boundary layer parameterization Reviews of Geophysics, *32*, 363–403.

Large W.G. and S.G. Yeager. 2004. Diurnal to decadal global forcing for ocean and sea-ice models: the data sets and flux climatologies. NCAR, Technical Note NCAR/ TN-460+STR, 111.

Levitus, S. 1998. Climatological atlas of the world ocean, Tech. Rep., NOAA, Rockville, Md.

McDougall T.J., D.R. Jacket, D.G. Wright and R. Feistel. 2003. Accurate and computationally efficient algorithms for potential temperature and density of seawater, J. Atm. Ocean. Tech., *20*, 730-741.

Murtugudde R., J.P. McCreary and A.J. Busalacchi. 2000. Oceanic processes associated with anomalous events in the Indian Ocean with relevance to 1997–1998. J. Geophys. Res., *105*, 3295–3306.

Nicholls N. 1989. Sea Surface temperatures and Australian winter rainfall, J. Clim., *2*, 965-973.

Pacanowski R.C. and A. Gnanadesikan. 1998. Transient response in a z-level ocean model that resolves topography with partial-cells, Mon. Wea. Rev, *126*, 3248-3270.

Rao S.A., S.K. Behera, Y. Masumoto and T. Yamagata. 2002. Interannual subsurface variability in the tropical Indian Ocean with a special emphasis on the Indian Ocean dipole, Deep Sea Res., Part II, *49*, 1549 – 1572.

Rao S.A. and T. Yamagata. 2004. Abrupt termination of Indian Ocean Dipole events in response to intraseasonal disturbances, Geophys. Res. Lett., *31*, L19306, doi:10.1029/2004GL020842.

Rao S. A. and S. K. Behera. 2005. Subsurface influence on SST in the tropical Indian Ocean: structure and interannual variability, Dynamics of Atmosphere and Oceans, *39*, 103-135.

Rayner N.A., D.E. Parker, E.B. Horton, C.K. Folland, L.V. Alexander, D.P. Rowell, E.C. Kent and A. Kaplan. 2003. Global analysis of sea surface temperature, sea ice, and night marine air temperature since the late nineteenth century, J. Geophys. Res., 108, D14, *4407*, doi:10.1029/2002JD002670.

Reverdin G. 1987. The upper equatorial Indian Ocean: the climatological seasonal cycle, J. Phys. Oceanogr., *17*, 903-927.

Saji N.H., B.N. Goswami, P.N. Vinayachandran and T. Yamagata. 1999. A dipole mode in the tropical Indian Ocean, Nature, *401*, 360-363.

Saji N.H. and T. Yamagata. 2003. Possible impacts of Indian Ocean dipole mode events on global climate, Clim. Res., *25*, 151-169.

Schott F. A. and J. P. McCreary Jr. 2001. The monsoon circulation of the Indian Ocean, Prog. Oceanogr., *51*, 1-123.

Shinoda T., H.H., Hendon and M.A., Alexander. 2004. Surface and subsurface dipole variability in the Indian Ocean and its relation with ENSO, Deep-Sea Res., *51*, 619-635.

Thompson B., C. Gnanseelan and P.S. Salvekar. 2005. Indian Ocean Dipole Simulation using Modular Ocean Model, I. I. T. M. Research Report, No RR-108.

Thompson B., C. Gnanaseelan and P. S. Salvekar. 2006. Variability in the Indian Ocean circulation and salinity and their impact on SST anomalies during dipole events, J. Mar. Res., 64, 853-880.

Vinayachandran P.N., S. Iizuka and T. Yamagata. 2002. Indian Ocean dipole mode events in an ocean General Circulation model, Deep Sea Res., Part II, *49*, 1573-1596.

Webster P.J., A.M. Moore, J.P. Loschnigg and R.R. Leben. 1999. Coupled ocean-atmosphere dynamics n the Indian Ocean during 1997-1998, Nature,*401*, 356-360.

Yu L. and M.M., Reinecker. 1999. Mechanism for the Indian Ocean warming during 1997-1998 El Nino, Geophys. Res. Lett., *26*, 735-738.

Yu L. and M.M., Reinecker. 2000. Indian Ocean warming of 1997-1998. J. Geophys. Res., *105*, 16923-16939.

Zubair L., S.A. Rao and T. Yamagata. 2003. Modulation of Sri Lankan Maha rainfall by the Indian Ocean Dipole, Geophys. Res. Lett., *30(2), 1063*, doi:10.1029/ 2002GL015639.

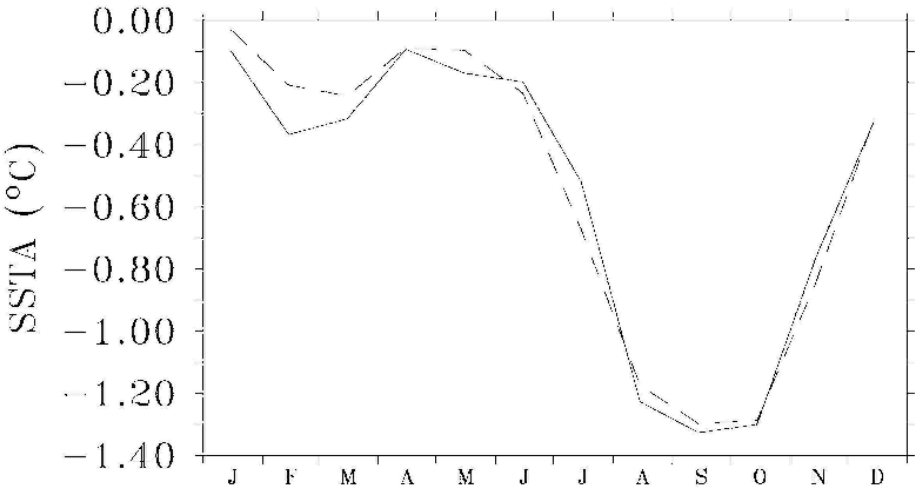

Figure 1. Composite evolution of SST anomalies over EEIO for the strong positive IOD years 1961, 1994 and 1997. Continuous line represent model and dash represents SODA.

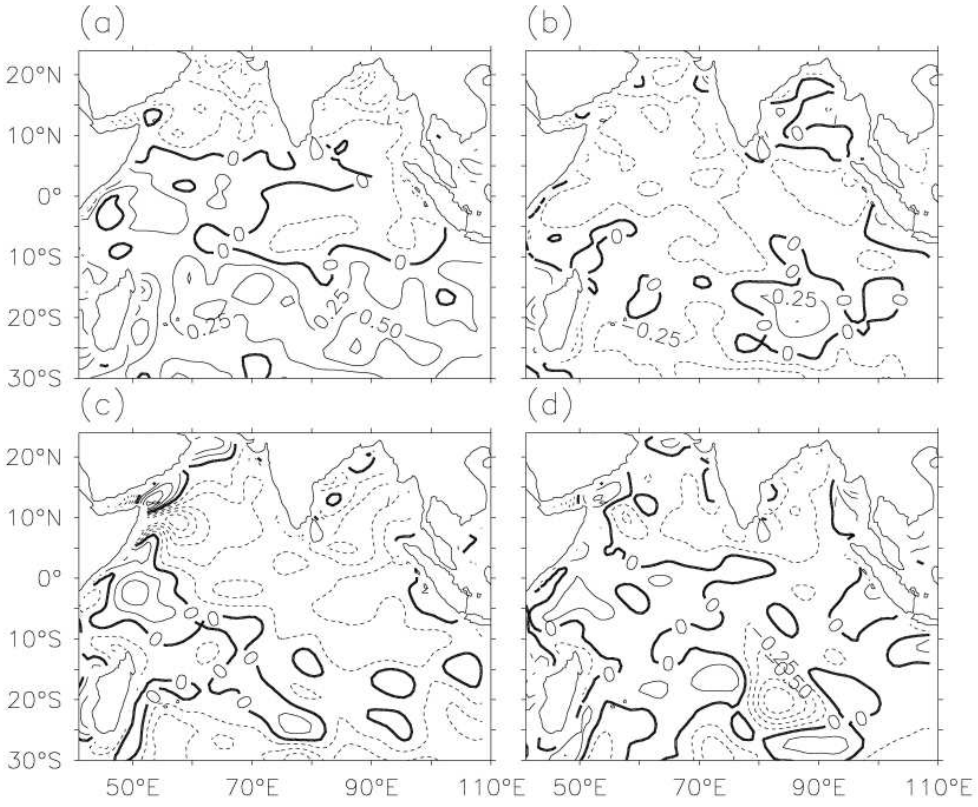

Figure 2. Difference between seasonal climatologies of model and Levitus (1998) for (a) winter, (b) spring, (c) summer and (d) fall seasons. The RMS differences are 0.37, 0.26, 0.37 and 0.31^{o}C for the respective seasons.

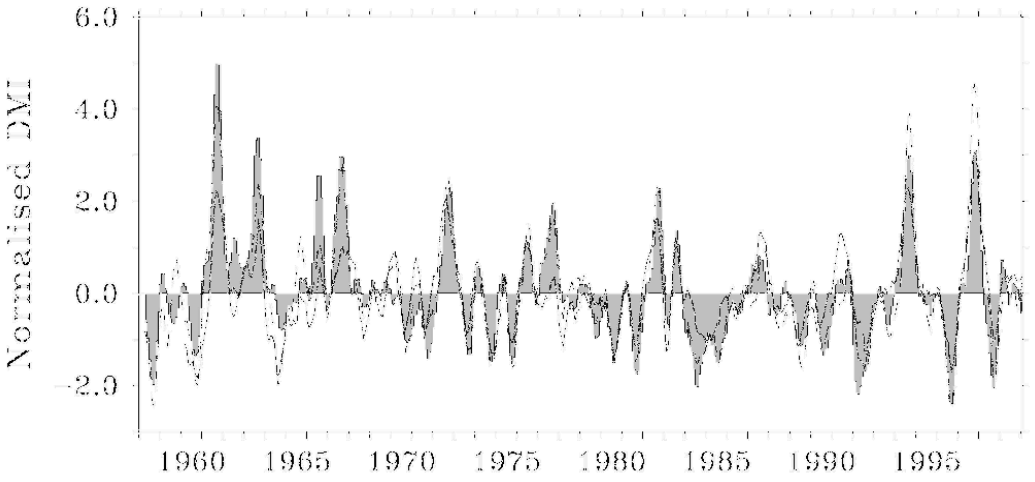

Figure 3. Dipole mode Index time series. Model (shaded), HadISST (continues line), SODA (dashed line).

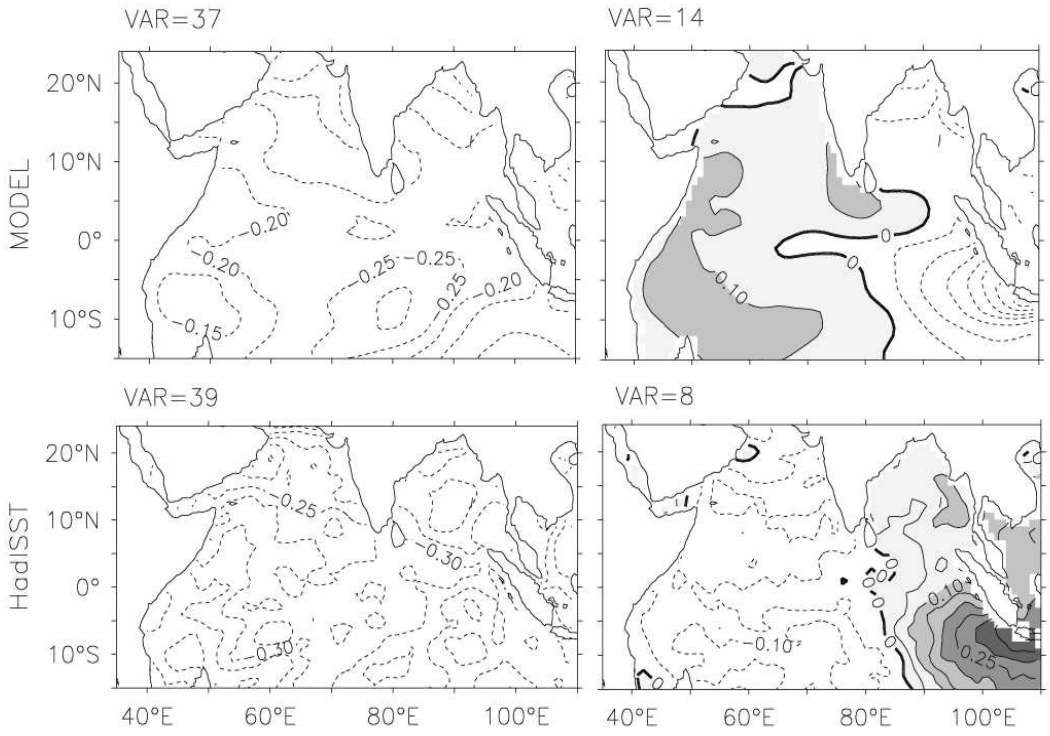

Figure 4. The spatial function of first (left panel) and second (right panel) leading EOF mode of SST anomalies from model (top panel) and HadISST (right Panel). EOF1 and EOF2 explain 37% and 14% of total variability for model and 39% and 8% for HadISST. Positive values are shaded.

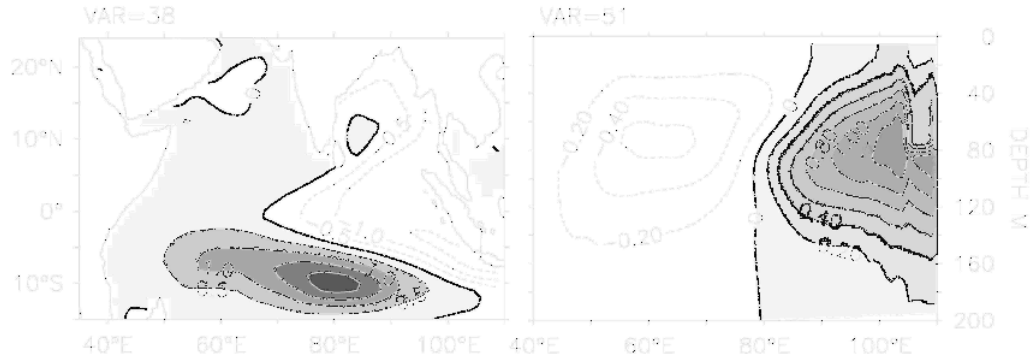

Figure 5. The spatial function of first leading EOF mode of temperature anomalies from model at 80 m depth (left panel) and in the longitude-depth plane, averaged over 10°S-5°N (right panel). It explains 38% and 51% of total variability respectively. Positive values are shaded.

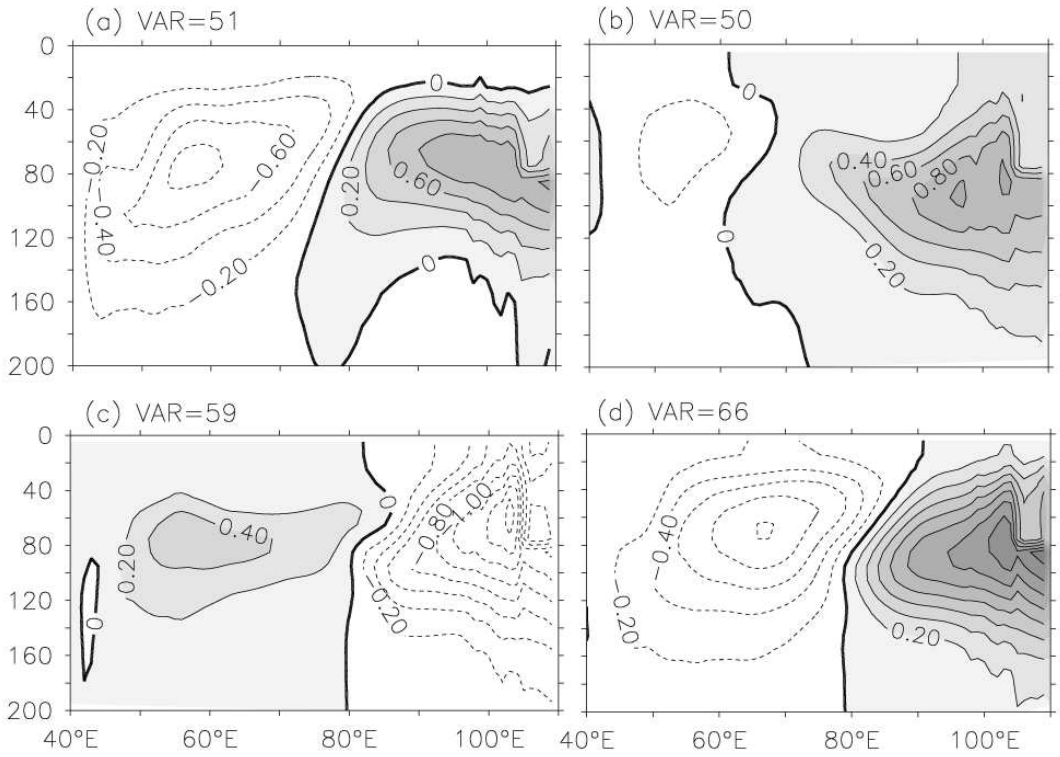

Figure 6. The spatial function of first leading EOF mode of temperature anomalies from model in the longitude-depth plane (averaged over 10°S-5°N) for (a) spring, (b) summer, (c) fall and (d) winter seasons. It explains 51%, 50%, 59% and 6% of total variability respectively. Shaded portion represent positive values.

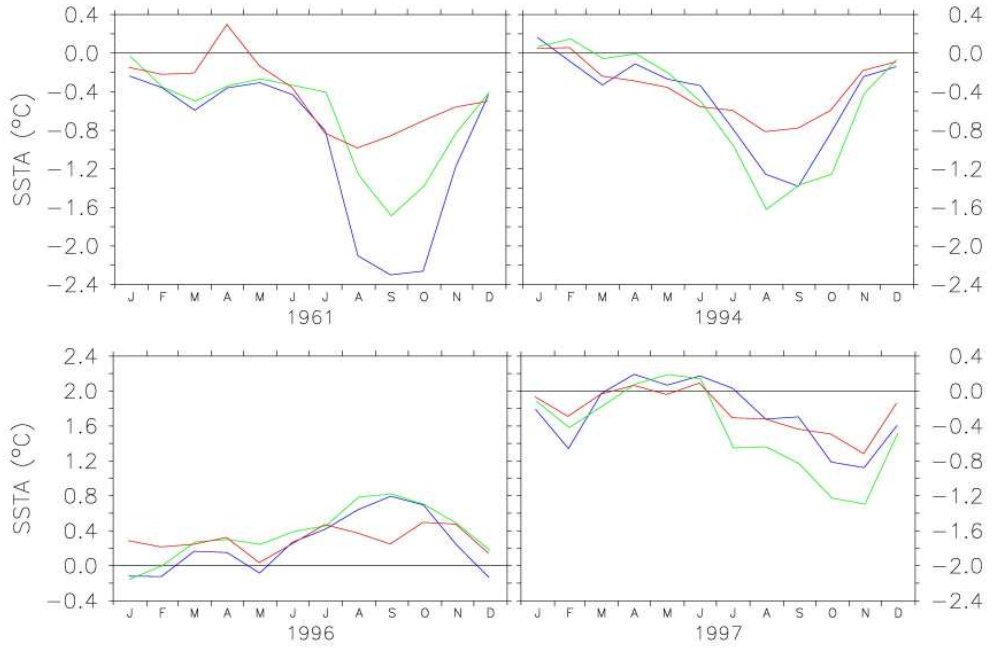

Figure 7. Evolution of SST anomalies over EEIO for 1961, 1994, 1996 and 1997. Model (blue line), SODA (green line) and HadISST (red line).

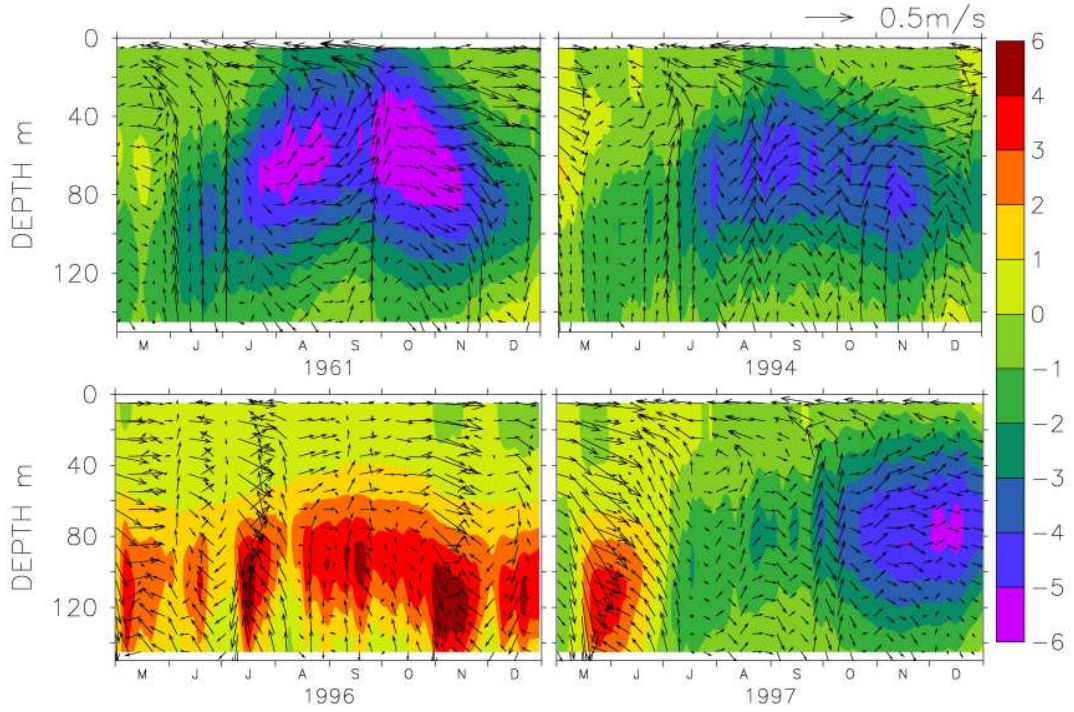

Figure 8. Time-Depth plot of subsurface temperature anomalies for 1961, 1994, 1996 and 1997. Zonal-Vertical current vectors are overlaid on temperature anomalies. The vertical currents are scaled up by 10000. Temperature anomalies and currents are averaged for 90°E to 110°E and 5°S to Equator.

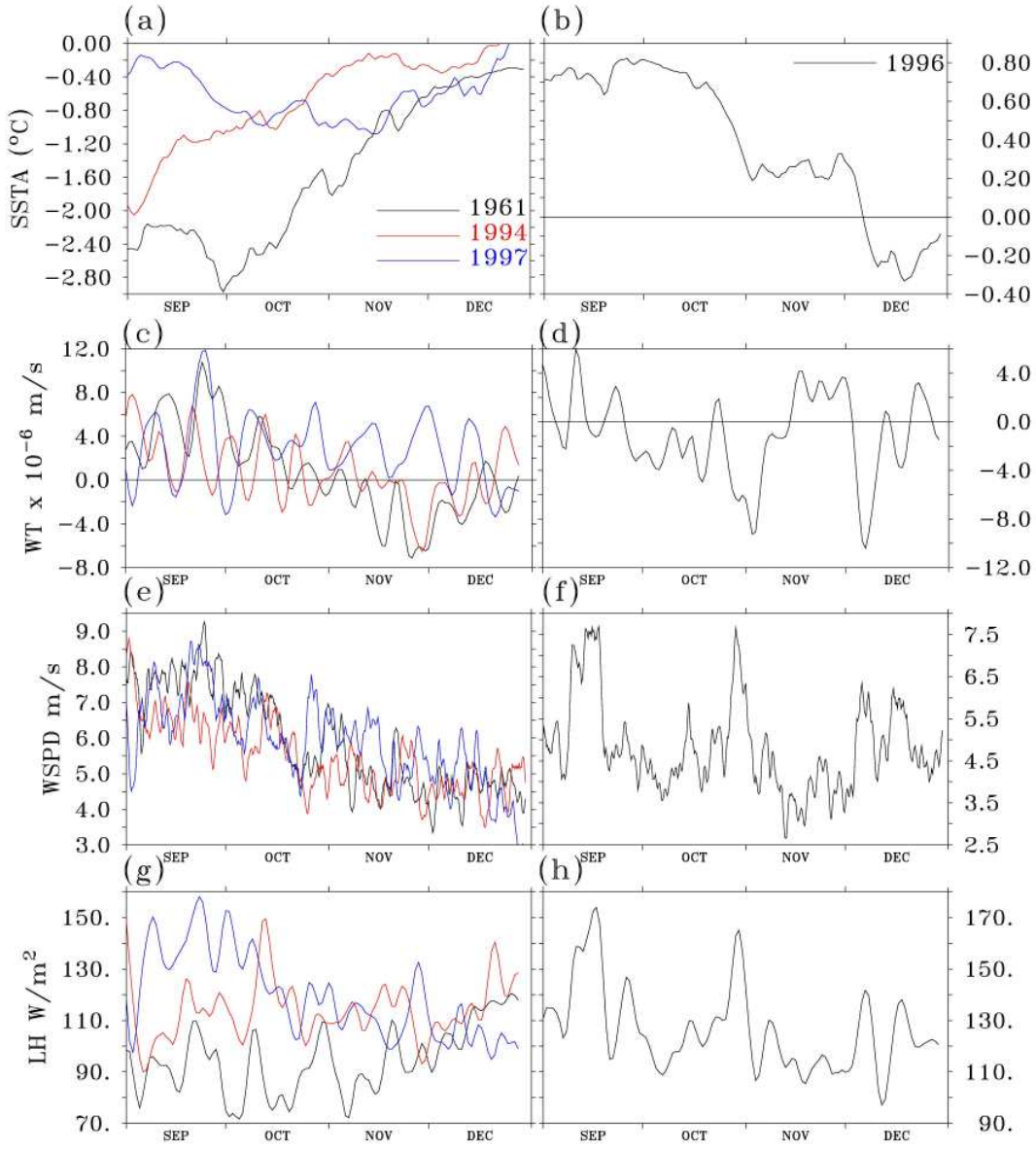

Figure 9. Termination of 1961, 1994, 1996 and 1997 IOD events. Left panel represents 1961 (black line), 1994 (red line) and 1997 (blue line) and right panel shows 1996 IOD termination phase. (SSTA - SST anomalies (model) ^{o}C, WT - Vertical velocity (model) at 50m (m/s), WSPD - surface wind speed (m/s), LH - Latent Heat flux calculated using model SST (W/m^2). All quantities are averaged for 90^{o}E to 110^{o}E and 10^{o}S to Equator.

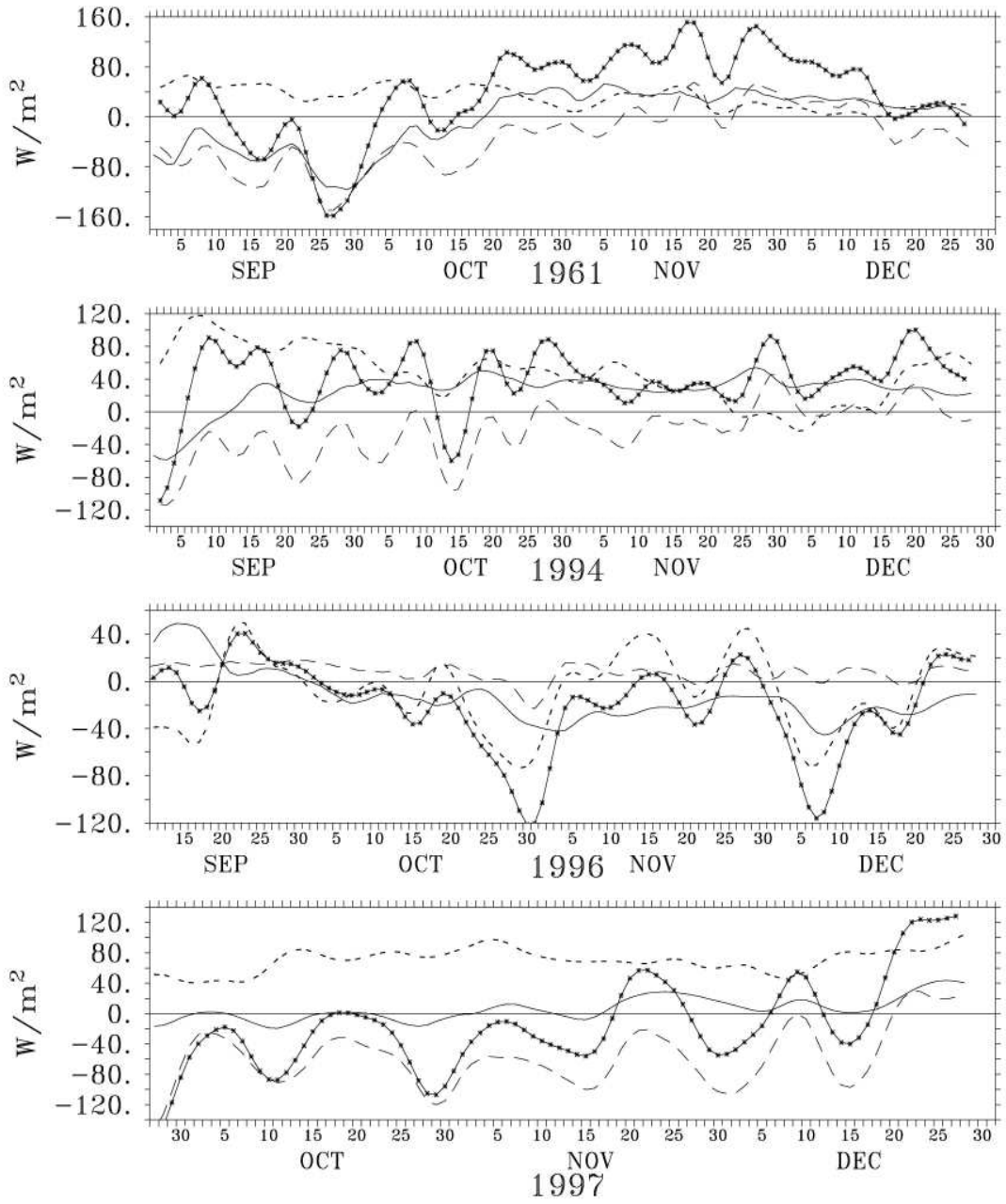

Figure 10. Anomalies of model 50m heat content tendency (marked continuous line), horizontal advection (continuous plain line) and vertical advection (dashed line) for upper 50m of the model and net surface heat flux (dotted line) in the EEIO during the termination phase of dipole mode years 1961, 1994, 1996 and 1997.

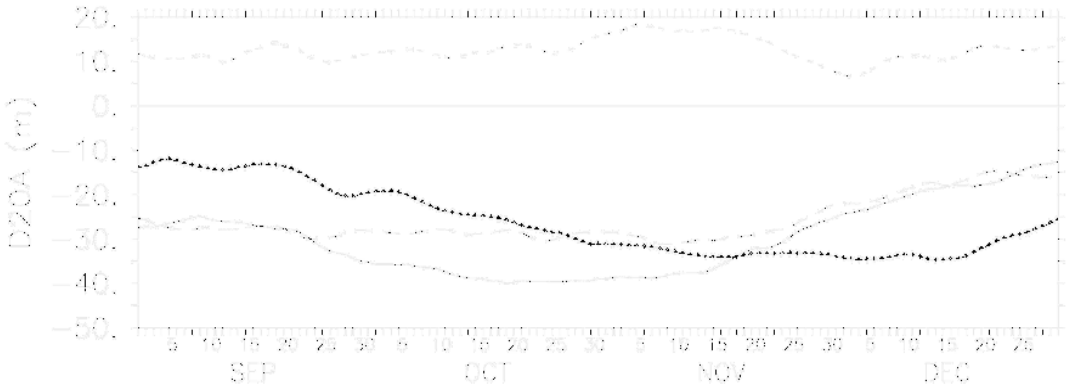

Figure 11. Depth of 20^{o}C isotherm anomaly from model in the EEIO during the termination phase of 1961 (continues line), 1994 (dashed line), 1996 (dotted line) and 1997 (marked line).